Colloidal diffusion over a quasicrystalline-patterned surface

Yun Su, Pik-Yin Lai, Bruce J. Ackerson, Xin Cao, Yilong Han, and Penger Tong

Citation: The Journal of Chemical Physics **146**, 214903 (2017); doi: 10.1063/1.4984938
View online: http://dx.doi.org/10.1063/1.4984938
View Table of Contents: http://aip.scitation.org/toc/jcp/146/21
Published by the American Institute of Physics

Colloidal diffusion over a quasicrystalline-patterned surface

Yun Su,[1] Pik-Yin Lai,[2] Bruce J. Ackerson,[3] Xin Cao,[1] Yilong Han,[1] and Penger Tong[1]
[1]*Department of Physics, Hong Kong University of Science and Technology, Clear Water Bay, Kowloon, Hong Kong*
[2]*Department of Physics and Center for Complex Systems, National Central University, Chungli District, Taoyuan City 320, Taiwan*
[3]*Department of Physics, Oklahoma State University, Stillwater, Oklahoma 74078, USA*

(Received 1 March 2017; accepted 19 May 2017; published online 7 June 2017)

We report a systematic study of colloidal diffusion over a substrate with quasicrystalline-patterned holes. Silica spheres of diameter comparable to the hole diameter diffuse over the patterned substrate and experience a gravitational potential $U(x, y)$. Using optical microscopy, we track the particle trajectories and find two distinct states: a trapped state when the particles are inside the holes and a free-diffusion state when they are on the flat surface outside the holes. The potential $U(x, y)$ and dynamic properties of the diffusing particle, such as its mean dwell time, mean square displacement, and long-time diffusion coefficient D_L, are measured simultaneously. The measured D_L is in good agreement with the prediction of two theoretical models proposed for diffusion over a quasicrystal lattice. The experiment demonstrates the applications of this newly constructed potential landscape. *Published by AIP Publishing.* [http://dx.doi.org/10.1063/1.4984938]

I. INTRODUCTION

Diffusion over a complex potential landscape is a common problem, which is found in many areas of physics, chemistry, and biology.[1–3] For example, the diffusion of lithium ions through the pores of a lithium ion battery affects the transport properties of the battery, and microstructural information of the battery is needed in order to quantify the ion transport.[4] In cell biology, membrane-bounded proteins in live cells were found to exhibit anomalous diffusion,[5–9] which results from a complex interaction landscape with the surrounding proteins and lipids and with the underlying cytoskeleton.[10–15] In the study of protein folding, the change of protein configurations is thought of as a diffusion in a funnel-like free energy landscape along the reaction coordinates.[16,17]

Owing to its fundamental importance, there have been a large number of theoretical studies of diffusion over regular lattices and disordered media.[1–3,15,18] Lifson and Jackson[19] obtained an exact solution of long-time diffusion over a one-dimensional (1D) periodic potential. While there is no exact solution available for diffusion over more complex potentials, various phenomenological models have been proposed to capture certain aspects of the actual potential encountered in the disordered media. These models include the random trap model,[20–22] random barrier model,[21–23] and continuous random walk model.[24–26] In these models, the diffusion of particles was assumed on a regular lattice, and randomness in the spatial arrangement of the diffusion obstacles has not been considered.

A quasicrystalline lattice lies in between regular periodic lattices and disordered media in that, while it lacks the long-range translational periodicity, the lattice sites in a quasicrystal still obey certain tiling rules so that they can be classified into groups according to their local arrangements.[27,28] Several numerical simulations have been carried out to study diffusion through quasicrystalline traps[29] and obstacles.[30] In contrast to the considerable theoretical and numerical studies, systematic experimental investigations of diffusion in quasicrystals are quite limited. Samavat *et al.* reported an experimental study of diffusion of atoms on a quasicrystalline alloy surface.[31] Guidoni *et al.* reported an experiment on atomic diffusion in an optical quasicrystal.[32] These experiments, however, were not conducted at the single particle level so that information about the particle trajectories is not available. This information is needed in order to find a relationship between the microscopic dynamics of particles and macroscopically measurable quantities, such as the long-time diffusion coefficient of the particles, in the theoretical predictions.

In this paper, we report a systematic experimental study of the diffusion dynamics of a dilute monolayer of micron-sized particles over a quasicrystalline-patterned surface. With the techniques of optical microscopy and particle tracking, we are able to obtain a large volume of single particle trajectories and the morphology of the quasicrystalline potential landscape that the individual particles have experienced. With the simultaneously obtained energetics and dynamics information, we test the theory and demonstrate the applications of the quasicrystalline potential landscape.

The paper is organized as follows. We first introduce two theoretical models for diffusion over a quasicrystalline-patterned substrate in Sec. II. The experimental setup and data analysis methods are described in Sec. III. The experimental results and discussion are given in Sec. IV. Finally, we summarize the work in Sec. V.

II. THEORY

A. Colloidal diffusion between two states

We consider the motion of a colloidal particle over a patterned substrate with identical holes arranged on a

quasicrystalline lattice (see Fig. 1 for the experimental setup). The holes on the substrate, whose size is comparable to the particle size, serve as traps to the diffusion of the colloidal particles. As shown in Fig. 3(b) below, the particle trajectories undergo two distinct states: a trapped state when the particles are inside the holes and a free-diffusion state when they are on the flat surface outside the holes. To describe the colloidal diffusion between the two states, we consider a two-state diffusion model with the coupled diffusion equations given by

$$\begin{aligned}\partial_t P_1(\mathbf{r},t) &= D_1\nabla^2 P_1(\mathbf{r},t) - k_1 P_1(\mathbf{r},t) + k_0 P_0(\mathbf{r},t),\\ \partial_t P_0(\mathbf{r},t) &= D_0\nabla^2 P_0(\mathbf{r},t) - k_0 P_0(\mathbf{r},t) + k_1 P_1(\mathbf{r},t),\end{aligned} \tag{1}$$

where $P_1(\mathbf{r}, t)$ $[P_0(\mathbf{r}, t)]$ is the probability density function of finding a particle in the trapped state [free-diffusion state] at position $\mathbf{r}$ and time t. In the above, D_1 and D_0 are the diffusion coefficients in the two states, and k_1 (k_0) is the transition rate for the particles to change their state $1 \to 0$ $(0 \to 1)$. Here we have assumed that colloidal diffusion between the two states is homogeneous in space and thus all the molecular parameters are constants independent of particle positions.

The motion of the particles over the quasicrystalline-patterned substrate can be described by the mean square displacement (MSD)

$$\langle \mathbf{r}^2(t)\rangle = \int \mathbf{r}^2\,[P_1(\mathbf{r},t) + P_0(\mathbf{r},t)]\,d\mathbf{r}, \tag{2}$$

under the initial conditions $P_1(\mathbf{r}, 0) = c_1\delta(\mathbf{r}), P_0(\mathbf{r}, 0) = c_0\delta(\mathbf{r})$, and $c_1 + c_0 = 1$, to let the particle start from the origin. When the distribution of the particles in the two states reaches equilibrium, we have

$$k_1 \int d\mathbf{r} P_1(\mathbf{r},t) = k_0 \int d\mathbf{r} P_0(\mathbf{r},t) \tag{3}$$

due to the detailed balance. If the initial state is already at equilibrium, we have $c_1/c_0 = k_0/k_1$. In this case, the MSD has a simple form

$$\langle \mathbf{r}^2(t)\rangle = 4\frac{D_0k_1 + D_1k_0}{k_1 + k_0}t = 4(D_L)_A t, \tag{4}$$

where the overall diffusion coefficient

$$(D_L)_A = c_0D_0 + c_1D_1, \tag{5}$$

which is just the average of the two diffusion coefficients weighted by the equilibrium number fraction of the particles in each state.

For a more general case, the MSD has the form

$$\langle \mathbf{r}^2(t)\rangle = 4\frac{D_0k_1 + D_1k_0}{k_1 + k_0}t + A\left(1 - e^{-(k_1+k_0)t}\right), \tag{6}$$

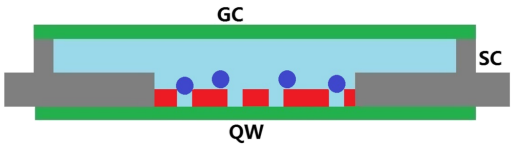

FIG. 1. Schematic diagram of the sample cell (side view): SC, stainless steel chamber; QW, quartz wafer; GC, glass cover slip; red layer with holes, SU8 photoresist layer with cylindrical holes arranged on a quasicrystal lattice; blue particles, silica spheres diffusing over the quasicrystalline-patterned substrate.

where

$$A = 4\frac{k_1c_1 - k_0c_0}{(k_1 + k_0)^2}(D_1 - D_0). \tag{7}$$

When the initial condition is at equilibrium, the second term vanishes and the MSD is reduced to Eq. (5). If it is initially not at equilibrium, $\langle \mathbf{r}^2(t)\rangle$ will undergo a transition between two diffusion regimes with the overall diffusion coefficient $(D_L)_A$ in Eq. (5) changed from its initial value to the final equilibrium value satisfying the detailed balance condition in Eq. (3). The crossover time is given by $1/(k_1 + k_0)$.

B. Colloidal diffusion on a quasicrystalline lattice

To further understand how the spatial location of the diffusion traps affects the overall diffusion dynamics, we consider the transition probability density function $P(\mathbf{R}_n, t|\mathbf{R}_l, t_0)$ for a particle starting from the site (hole) $\mathbf{R}_l$ at time $t_0 = 0$ to reach the site (hole) $\mathbf{R}_n$ at time t. Hereafter, we drop the initial time t_0 for simplicity. The evolution of $P(\mathbf{R}_n, t|\mathbf{R}_l, t_0)$ can be described by the master equation[1]

$$\frac{d}{dt}P(\mathbf{R}_n,t|\mathbf{R}_l) = \sum_m \Gamma_{m,n}P(\mathbf{R}_m,t|\mathbf{R}_l) - \sum_m \Gamma_{n,m}P(\mathbf{R}_n,t|\mathbf{R}_l), \tag{8}$$

where $\Gamma_{n,m}$ is the transition rate from site $\mathbf{R}_n$ to site $\mathbf{R}_m$, and $\sum_m$ denotes a sum over all the possible transitions from the neighbouring site m to the site n. In the Fourier $(\mathbf{k})$ space, Eq. (8) can be written as

$$\begin{aligned}\frac{d}{dt}P(\mathbf{k},t) = &\sum_m P(\mathbf{R}_m,t|\mathbf{R}_l)e^{-i\mathbf{k}\cdot(\mathbf{R}_m-\mathbf{R}_l)}\sum_n \Gamma_{m,n}e^{-i\mathbf{k}\cdot(\mathbf{R}_n-\mathbf{R}_m)}\\ &- \sum_n P(\mathbf{R}_n,t|\mathbf{R}_l)e^{-i\mathbf{k}\cdot(\mathbf{R}_n-\mathbf{R}_l)}\sum_m \Gamma_{n,m},\end{aligned} \tag{9}$$

where

$$P(\mathbf{k},t) = \sum_n P(\mathbf{R}_n,t|\mathbf{R}_l)e^{-i\mathbf{k}\cdot(\mathbf{R}_n-\mathbf{R}_l)} \tag{10}$$

is the Fourier transform of $P(\mathbf{R}_n, t|\mathbf{R}_l)$.

It is difficult to solve Eq. (9) because $\Gamma_{m,n}$ depends on both the starting site m and ending site n. For a quasicrystal, one cannot classify the neighboring site pairs into a finite number of groups as one does for a non-Bravais periodic lattice. To reduce the statistical complexities of $\Gamma_{m,n}\exp[-i\mathbf{k}\cdot(\mathbf{R}_n-\mathbf{R}_m)]$, we introduce a spatial average over all the starting sites m, so that $\Gamma_{m,n}\exp[-i\mathbf{k}\cdot(\mathbf{R}_n - \mathbf{R}_m)]$ becomes independent of m. In this case, we have

$$\Lambda(\mathbf{k}) = \sum_n \langle \Gamma_{m,n}[e^{-i\mathbf{k}\cdot(\mathbf{R}_n-\mathbf{R}_m)} - 1]\rangle_m. \tag{11}$$

In the above, the average $\langle \ldots\rangle_m$ over the starting sites m retains the essential symmetry of the quasicrystal but removes the minor differences among different sites of the quasicrystal. This average will also improve the statistics of the measurement (see more discussions in Sec. IV B). With Eq. (11), Eq. (9) is simplified to

$$\frac{d}{dt}P(\mathbf{k},t) = \Lambda(\mathbf{k})P(\mathbf{k},t), \tag{12}$$

which has a solution

$$P(\mathbf{k},t) = e^{\Lambda(\mathbf{k})t}, \tag{13}$$

under the initial condition, $P(\mathbf{R}_n, 0|\mathbf{R}_l) = \delta(\mathbf{R}_n - \mathbf{R}_l)$, at $t = 0$.

The MSD can be calculated using Eqs. (10)–(13), and the final result is given by

$$\langle \Delta \mathbf{R}^2(t) \rangle = -\nabla_{\mathbf{k}}^2 P(\mathbf{k}, t)|_{\mathbf{k}=0} = \sum_n \langle (\Delta \mathbf{R}_{m,n})^2 \Gamma_{m,n} \rangle_m t$$
$$= 4(D_L)_B t, \tag{14}$$

where

$$(\Delta \mathbf{R}_{m,n})^2 = (\mathbf{R}_n - \mathbf{R}_m)^2 \tag{15}$$

and

$$(D_L)_B = \frac{1}{4} \sum_n (\Delta \mathbf{R}_n)^2 \langle \Gamma_{m,n} \rangle_m. \tag{16}$$

In the above, $\Delta \mathbf{R}_n$ denotes all possible displacement vectors on the quasicrystal substrate, and $\langle \Gamma_{m,n} \rangle_m$ is the averaged value of $\Gamma_{m,n}$ over all starting sites m. Because $\langle \Gamma_{m,n} \rangle_m$ is independent of m, we find $\langle (\Delta \mathbf{R}_{m,n})^2 \Gamma_{m,n} \rangle_m = (\Delta \mathbf{R}_n)^2 \langle \Gamma_{m,n} \rangle_m$.

C. Connections between the two models

In the first model presented in Sec. II A, we ignored the spatial arrangement of the trapping sites and only considered the mixing effect of the two-state motion, which is used to calculate the long-time diffusion coefficient $(D_L)_A$. In the second model presented in Sec. II B, the long-time diffusion coefficient $(D_L)_B$ was derived from the local transition rates (or connectivity) between the neighbouring sites. The connection between the two models can be found when Eq. (4) is written as

$$\langle \mathbf{r}^2(t) \rangle = 4 \frac{D_0 \bar{t}_0 + D_1 \bar{t}_1}{\bar{t}_0 + \bar{t}_1} t = [\langle \mathbf{r}_0^2 \rangle + \langle \mathbf{r}_1^2 \rangle] N \Gamma t, \tag{17}$$

where $\bar{t}_0 = 1/k_0$, $\bar{t}_1 = 1/k_1$, and $\langle \mathbf{r}_0^2 \rangle = 4 D_0 \bar{t}_0$ and $\langle \mathbf{r}_1^2 \rangle = 4 D_1 \bar{t}_1$ are, respectively, the mean squared travelling distances in the free and trapped states. In the above, $\Gamma = \sum_n \langle \Gamma_{m,n} \rangle_m$ is the total transition rate for a particle to escape from a trapping site and arrive at all possible neighbouring sites, and N is defined by

$$1/\Gamma = N(\bar{t}_0 + \bar{t}_1). \tag{18}$$

When the particle escapes from a trap, it has a certain probability to come back to the same trap again. This escape-and-retrapping process may repeat several times until the particle is trapped at another site. In Eq. (18), $\bar{t}_0 + \bar{t}_1$ is the average time needed for a particle to make a transition. This time is shorter than the real transition time $1/\Gamma$ to a different site, because $\bar{t}_0 + \bar{t}_1$ includes the "self-transition" (escape-and-retrapping) events. Therefore, N in Eq. (18) represents the mean repeated number of the (self) transition events needed for a real transition to occur. Both N and $\langle \mathbf{r}_0^2 \rangle$ depend on the detailed arrangement of the trapping sites and trap size $\langle \mathbf{r}_1^2 \rangle$.

By comparing Eq. (17) with Eq. (14), we find that the predicted long-time diffusion coefficients, $(D_L)_A$ and $(D_L)_B$, become equal if

$$\langle (\Delta \mathbf{R}_n)^2 \rangle \equiv \sum_n (\Delta \mathbf{R}_n)^2 \frac{\langle \Gamma_{m,n} \rangle_m}{\Gamma} = (\langle \mathbf{r}_0^2 \rangle + \langle \mathbf{r}_1^2 \rangle) N. \tag{19}$$

Equation (19) is a statement in space with a meaning similar to Eq. (18). Here $\langle \mathbf{r}_0^2 \rangle + \langle \mathbf{r}_1^2 \rangle$ is the mean squared travelling distance needed for a particle to make a transition, which includes the self-transition event. It needs to be repeated N times in order to reach the value of $\langle (\Delta \mathbf{R}_n)^2 \rangle$ for a real transition to a different site. In Sec. IV, we will compare the experimental results with the predictions given by Eqs. (5) and (16), which are obtained by two different statistical approaches.

III. EXPERIMENT

A. Apparatus and sample preparation

Figure 1 shows the sample cell used in the experiment. It has a circular stainless steel chamber (SC) with a central hole of 8 mm in diameter and 1 mm in depth, which is sealed from the bottom by a quartz wafer (QW). A quasicrystalline-patterned substrate is coated on the bottom quartz wafer. The central hole is then filled with the colloidal sample and extra solvent (water) is added to fill the entire sample cell. After filling the fluid chamber, another glass cover (GC) slip is used to cover the entire sample cell. In this way, both sample evaporation and unwanted flow are minimized.

The quasicrystalline pattern is etched on a thin layer of SU8 photoresist coated on a quartz wafer. It contains identical cylindrical holes of diameter d_h, which are arranged on a quasicrystal lattice. These cylindrical holes are made by photolithography. The quasi-crystalline pattern is first created using the generalized dual method[33] and then transferred onto a mask using a laser direct write system (Intertech ISI-2808) under the bright field. A photoresist layer of 0.5 μm in thickness (SU-8 2000.5) covered with the mask is exposed to an UV light, and the unexposed photoresist is then dissolved away with an SU-8 developer. The depth of the resulting cylindrical holes is the same as the photoresist layer thickness.

Figure 2(a) shows a microscopic image of the sample surface. Because the resolution of photolithography is limited to ~1 μm, the holes on the quasicrystalline-patterned substrate are not perfectly cylindrical, and variations in the hole depth are observed over large scales across the entire area of the wafer. By laterally moving the sample stage, we are able to find individual patches within the view area of 100 $\times$ 75 μm^2, which are uniform enough so that the experimental results to be discussed below are not affected by the sample imperfections.

As shown in Fig. 2(b), the quasicrystalline lattice has five-fold symmetry and can be constructed by tiling the surface with two kinds of rhombuses [two-dimensional (2D) Penrose tiling]. The two rhombuses have the same length of edges but with different diagonals. The three colored links represent the three shortest distances between the neighbouring holes. Because of the quasicrystalline nature, each hole has its own unique neighborhood if all the surrounding holes are considered.

The colloidal sample preparation and image analysis procedures used in the experiment are similar to those described in Refs. 34 and 35. Briefly, silica spheres (Bangs Laboratories) are first thoroughly washed by deionized water. We then prepare dilute suspensions of monodispersed silica spheres of diameter d_p. When the suspension is filled into the central hole of the fluid chamber (~50 μl in volume), the particles settle on the quasicrystalline-patterned substrate under gravity

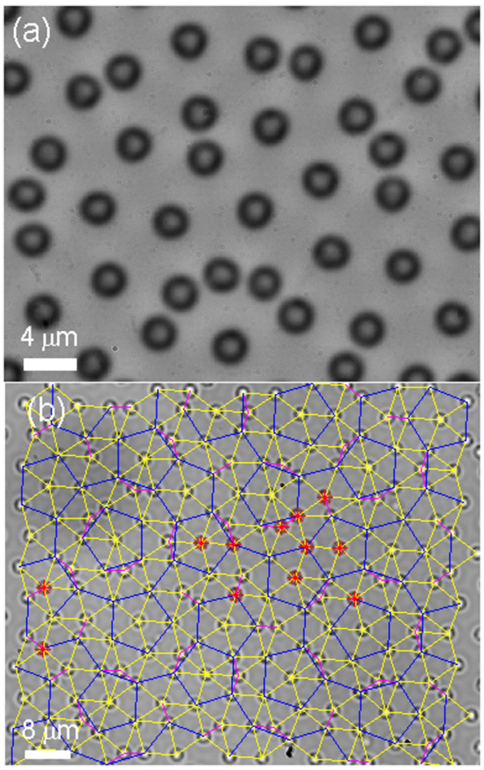

FIG. 2. (a) A microscopic image of the quasicrystalline-patterned substrate for S4 with cylindrical holes arranged on a quasicrystal lattice. (b) 2D-Penrose tiling of the quasicrystal lattice, on which the cylindrical holes (small circles) are arranged. The quasicrystal lattice is constructed by tiling the surface with two kinds of rhombuses. The yellow lines show the edges of the rhombuses. The blue lines show the shorter diagonal of the fat rhombus. The pink lines show the shorter diagonal ℓ_h of the thin rhombus, which is used as a characteristic length of the quasicrystal. The red stars indicate 12 different kinds of vertices formed by the three colored links.

and form a monolayer with area fraction n_A, which is defined as the ratio of the occupied area by the particles to the total area. In the experiment, n_A is in the range of 0.015-0.040, in which the interactions between the silica spheres can be ignored.[34,35]

The silica spheres diffuse over a rugged surface of the quasicrystalline-patterned substrate and experience a gravitational potential $U(x, y)$. The values of $U(x, y)$ are determined by both the size d_p of the diffusing particles and the hole diameter d_h.[34] There is a small gap between the silica spheres and substrate, which affects both the diffusion dynamics of the particles and the potential field $U(x, y)$. To obtain consistent experimental results, we add 2 mM sodium dodecyl sulfate (0.8 mM for sample S2) into the solution to prevent the particles from sticking to the substrate and to control the Debye screening length of the silica spheres so that the gap distance maintains constant. To vary $U(x, y)$, we change the size d_p of the silica spheres and the parameters of the quasicrystal structure, such as the hole diameter d_h and shorter diagonal ℓ_h of the thin rhombus. Five samples are used in the experiment, and their properties are given in Table I.

B. Image processing

The sample cell is placed on the stage of an inverted microscope (Olympus IX71). The motion of the particles over the (transparent) quasicrystalline-patterned substrate is viewed from below using bright field microscopy and recorded by a CMOS camera (acA1920-155um, Basler). A typical frame rate used is 10 frames per second (fps). The recorded images have a spatial resolution of 1920 × 1080 pixels and 256 gray scales.

Figure 3(a) shows the silica spheres (bright dots) of sample S4 diffusing over the quasicrystalline-patterned substrate. Because the substrate is slightly off focus, the image of the holes on the substrate appears as dark rings. The intensity profile of the diffusing particles is not always uniform due to the optical interference with the bottom holes. By applying a standard Gaussian filter to the original image, one can recover the uniform Gaussian-like intensity profile for each diffusing particle.[34] The center of this intensity profile is defined as the position of the particle. A homemade program based on the standard tracking algorithm[36] is used to find the trajectory of the diffusing particles from consecutive images. With this program, we are able to obtain a tracking accuracy of 1 pixel ≃ 97.6 nm. By adding all the images in the same movie together, we average out the individual image of the randomly positioned particles and obtain a clear picture of the substrate, from which we identify the position of the holes on the substrate.

Figure 3(b) shows three representative trajectories of the diffusing particles over the quasicrystalline-patterned substrate for sample S4. The particle's trajectories show two distinct states: a trapped state when the particles are inside the holes and a free-diffusion state when they are on the flat substrate outside the holes. Thus the particle trajectories are divided into trapped segments and free-diffusion segments. From the center of the holes on the substrate, we define a trap diameter d_{tr} for each sample, which is about the same as the hole diameter d_h. All the particle trajectories inside the

TABLE I. Five samples used in the experiment with different particle diameters d_p and area fractions n_A on a quasicrystalline substrate with different hole diameters d_h and shortest distances ℓ_h between the holes. Also shown are the measured quantities from the particle trajectories, including the free diffusion coefficient D_0, trap radius r_1, mean dwell time $\bar{t}_1$ in the trapped state, mean dwell time $\bar{t}_0$ in the free-diffusion state, particle number ratio n_0/n_1 between the free diffusion and trapped states, potential barrier E_b/k_BT of the traps, and long-time diffusion coefficient D_L.

Sample	d_p (μm)	d_h (μm)	ℓ_h (μm)	n_A	D_0 (μm^2/s)	r_1 (μm)	$\bar{t}_1$ (s)	$\bar{t}_0$ (s)	n_0/n_1	E_b/k_BT	D_L (μm^2/s)
S1	2.01	2.4	3	0.039	0.120	1.058	3.76	10.23	2.498	1.1	0.110
S2	2.49	2.4	3	0.028	0.091	1.155	7.38	7.74	1.049	2.1	0.067
S3	2.49	2.4	3	0.018	0.119	0.732	12.03	5.63	0.561	3.2	0.051
S4	2.49	3.2	4	0.021	0.089	1.013	45.02	10.67	0.254	4.2	0.023
S5	2.49	3.6	4	0.015	0.117	1.134	123.3	7.55	0.057	5.8	0.012

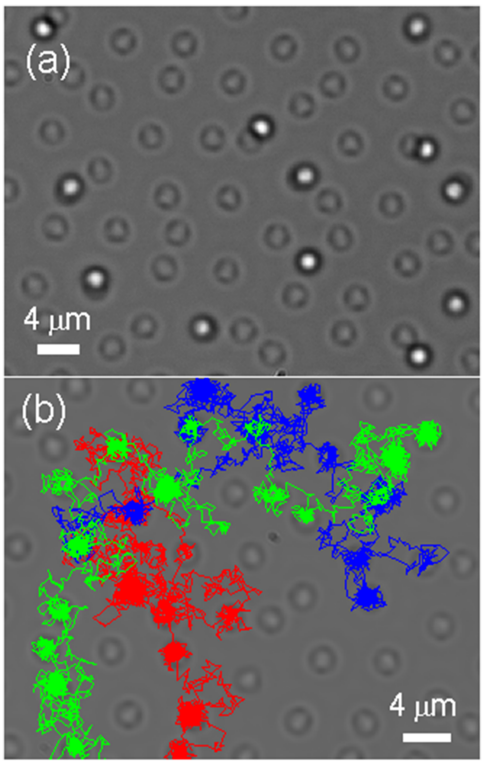

FIG. 3. (a) Microscopic image of sample S4. Bright dots are the diffusing particles. The dark rings arranged as a quasicrystalline lattice are the holes on the substrate, which are slightly below the focal plane. (b) Three representative particle trajectories (red, blue, and green) over a time period of 1.94 h for sample S4. Brighter dots are the cylindrical holes on the substrate.

traps of diameter d_{tr} are labelled as trapped segments, and the other segments of the trajectories are labelled as free-diffusion segments. The value of d_{tr} is slightly adjusted to minimize the number of short trajectories resulting from rapid crossings of the trap boundary due to thermal fluctuations.

IV. EXPERIMENTAL RESULTS

A. Diffusion dynamics between two states

From the particle trajectory, we obtain the probability density function (PDF) $P(x, y)$ of finding a particle at location (x, y) inside a trap, which is related to the trap potential $U(x, y)$ by the Boltzmann distribution, $U(x, y)/k_BT = -\ln P(x, y)$. Here $P(x, y)$ is normalized in such a way that $U(x, y) = 0$ at the flat surface of the substrate. Figure 4 shows a 3D plot of the obtained trap potential, $U(x, y)/k_BT$, for sample S3. The shape and symmetry of the measured $U(x, y)$ reflect the topographic variation of the cylindrical holes explored by the particles with a finite radius. It is seen that the potential barrier E_b of the traps for sample S3 is $E_b \simeq 3.2\, k_BT$.

The duration of a trapped segment of the particle trajectory gives the dwell time t_1 (also called "escape time"). Figure 5 shows the measured histogram $H(t_1)$ of the dwell time t_1 (black curve) for sample S3. It has a long tail, which is well described by a simple exponential function, $H(t_1) = 0.0692 \exp(-t_1/\bar{t}_1)$ with $\bar{t}_1 \simeq 12$ s (red dashed line). This result suggests that the escape events from the holes occur randomly in time and can be described by a Poisson process with a constant escape rate $k_1 = 1/\bar{t}_1$.[37] Similarly, we measure the dwell time t_0 for

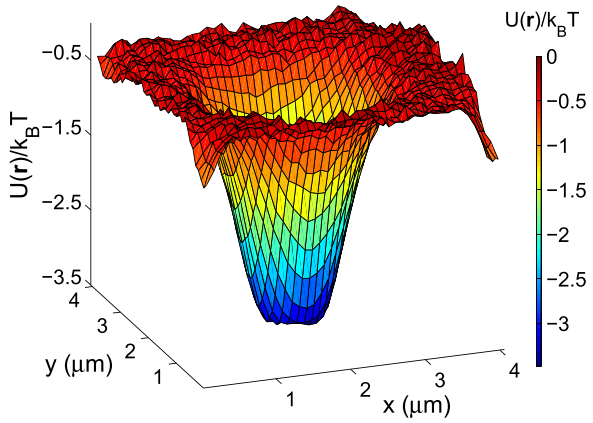

FIG. 4. 3D plot of the obtained trap potential, $U(x, y)/k_BT = -\ln P(x, y)$, for sample S3. Approximately 500 trapped trajectories are used to compute $P(x, y)$.

the particles in the free-diffusion state. The green curve in Fig. 5 shows its normalized histogram $H(t_0)$. The measured $H(t_0)$ is not a simple exponential function, indicating that the transition rate $k_0 = 1/\bar{t}_0$ out of the free-diffusion state is not a constant. This is because when a particle diffuses over the flat surface of the substrate, there is no characteristic time for the particle to reach the holes. The value of t_0 depends on the initial position of the particle and the local arrangement of the holes. In the above, the mean value of t_0 is defined as $\bar{t}_0 = \sum t_0 H(t_0) / \sum H(t_0)$. The measured $H(t_1)$ [and $H(t_0)$] near the origin shows a slight curve-up, which is caused by the experimental uncertainties in determining the actual location of the trap boundaries, as mentioned above.

As discussed in Sec. II A, when the distribution of the particles in the two states reaches equilibrium, one has

$$\frac{\bar{t}_1}{\bar{t}_0} = \frac{n_1}{n_0} \tag{20}$$

due to the detailed balance. Here n_1/n_0 is the number ratio of the particles in the two states, which can be independently measured from the particle trajectories. Figure 6 shows the measured ratio $\bar{t}_1/\bar{t}_0$ of the two mean dwell times as a function of number ratio n_1/n_0. The data are well described by Eq. (20) (solid line), suggesting that the distribution of the particles in the two states has already reached equilibrium.

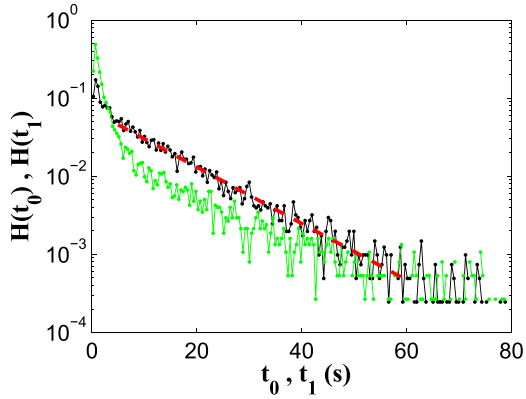

FIG. 5. Measured histograms $H(t_1)$ of the dwell time t_1 in the trapped state (black curve) and $H(t_0)$ of the dwell time t_0 in the free-diffusion state (green curve) for sample S3. The red dashed line is an exponential fit, $H(t_1) = 0.0692 \exp(-t_1/12\ \text{s})$, to the tail part of the measured $H(t_1)$.

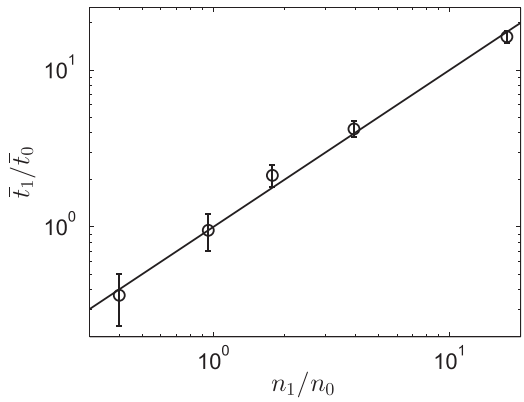

FIG. 6. Measured ratio $\bar{t}_1/\bar{t}_0$ of the two mean dwell times as a function of number ratio n_1/n_0 of the particles in the two states. The error bars show the standard deviation of the measured $\bar{t}_1/\bar{t}_0$. The solid line is a plot of Eq. (20) with a slope of unity.

From the particle trajectories, we calculate the MSD $\langle \Delta \mathbf{r}^2(\tau) \rangle$ as a function of delay time τ, where $\Delta \mathbf{r} = \mathbf{r}(t+\tau) - \mathbf{r}(t)$. Figure 7 shows the measured MSD $\langle \Delta \mathbf{r}^2(\tau) \rangle$ as a function of τ for sample S5. The MSD curves are obtained under different sampling conditions. The red curve is obtained from the free diffusion segments. Indeed, the red curve is a typical MSD for free Brownian diffusion with a linear dependence on τ over the entire range of delay times sampled. From the intercept of this log-log plot of the MSD curve, we obtain the free diffusion coefficient D_0 for sample S5. The blue curve is obtained from the trapped segments. It is a linear function of τ for small delay times with $\tau < \tau_c$ and then reaches a plateau value r_1^2, which characterizes the size of the trap. This is a typical MSD curve for confined diffusion with the crossover time $\tau_c \simeq r_1^2/(4D_0')$ (left arrow). Here D_0' is the short-time diffusion coefficient inside the trap, which is slightly smaller than D_0 in the free-diffusion state (see the intercept of the blue curve).

The black curve in Fig. 7 is obtained from the full trajectories of sample S5. This MSD curve can be generally described by[15,18]

$$\langle \Delta r^2(\tau) \rangle \sim \tau^{\gamma}, \tag{21}$$

where the exponent γ is used to classify the particle's motion as normal diffusion ($\gamma = 1$), sub-diffusion ($\gamma < 1$), or super-diffusion ($\gamma > 1$). It is found that for short delay times with $\tau < \tau_c$, the motion of the particles (in both states) is diffusive with $\gamma = 1$ (lower left dashed line) and the overall diffusion coefficient is just the average of the diffusion coefficients in the two states weighted by the equilibrium number fraction of the particles in each state. At long delay times with $\tau > \bar{t}_1$ (right arrow), the particles have escaped from the traps, and their motion becomes diffusive again with $\gamma = 1$ (upper right dashed line). In this case, we find

$$\langle \Delta \mathbf{r}^2(\tau) \rangle = 4D_L\tau, \tag{22}$$

where D_L is the long-time diffusion coefficient, which is smaller than D_0. In the crossover region $\tau_c \lesssim \tau \lesssim \bar{t}_1$, the particle's motion becomes heterogeneous and undergoes sub-diffusion with $\gamma < 1$. Such a crossover behavior of MSD has been observed previously for colloidal diffusion over the periodic and random potentials[34,38,39] and in dense fluid systems, such as colloidal diffusion near its glass transition[40,41] and in entangled actin filament networks.[42] Membrane proteins in live cells were also found to exhibit anomalous subdiffusion.[5,9]

As shown in Fig. 8, the crossover regime of the obtained MSD curves from the full particle trajectory becomes less prominent when the traps are weaker. The energy barrier associated with the traps varies among different samples, as the effective depth that a particle can fall into the hole varies with both the hole diameter d_h and particle diameter d_p. For the particles with $d_p > d_h$, the larger the hole diameter is, the deeper the particles can fall into the holes. As a result, the samples with a larger hole diameter generally have a stronger trap in this experiment. By comparing the measured MSD curves from different samples, we find that the anomalous subdiffusion becomes more pronounced for the colloidal samples with stronger traps. The range of the crossover regime is also increased for the samples with stronger traps. The values of the measured free diffusion coefficient D_0, trap radius r_1, mean dwell times $\bar{t}_1$ and $\bar{t}_0$, particle number ratio n_0/n_1, potential barrier E_b/k_BT, and long-time diffusion coefficient D_L for all five

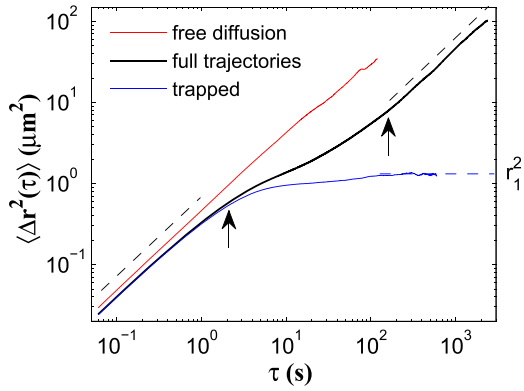

FIG. 7. Log-log plots of the measured MSD $\langle \Delta \mathbf{r}^2(\tau) \rangle$ as a function of delay time τ for sample S5. The MSD curves are obtained under different sampling conditions: (i) from the free diffusion segments (red curve), (ii) from the full trajectories (black curve), and (iii) from the trapped segments (blue curve). The black dashed lines indicate the relationship $\langle \Delta \mathbf{r}^2(\tau) \rangle \sim \tau$ with a slope of unity in the log-log plot. The horizontal blue dashed line indicates the plateau value r_1^2 of the blue curve. The two arrows point to the locations of τ_c (left arrow) and $\bar{t}_1$ (right arrow), respectively.

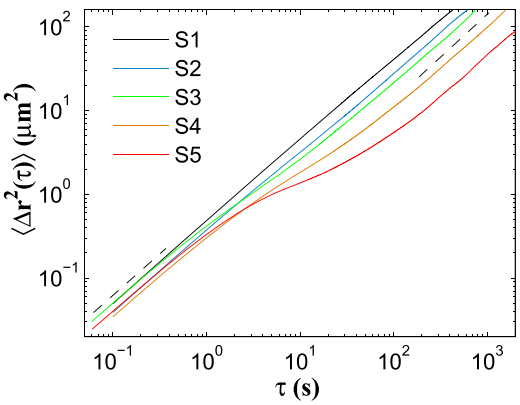

FIG. 8. Log-log plots of the measured MSD $\langle \Delta \mathbf{r}^2(\tau) \rangle$ as a function of delay time τ for five colloidal samples. The MSD curves are obtained from the full trajectory of the particles. The black dashed lines indicate the relationship $\langle \Delta \mathbf{r}^2(\tau) \rangle \sim \tau$ with a slope of unity in the log-log plot.

samples are given in Table I. Note that the measured values of D_L for the quasi-crystalline substrate here are in general larger than those for the periodic substrate with similar values of E_b in Ref. 34. This is because there is a significant fraction of flat regions on the quasi-crystalline substrate, on which the particle diffuses freely, whereas the periodic potential in Ref. 34 is made by a close-packed colloidal substrate, on which the particle does not experience free diffusion.

We now compare the measured long-time diffusion coefficient D_L with the theoretical prediction given in Eq. (5). With the measured quantities given in Table I, we rewrite Eq. (5) as

$$(D_L)_A = c_0\,[D_0 + (c_1/c_0)D_1] = \frac{n_0}{n_1+n_0}\left(D_0 + \frac{n_1}{n_0}\frac{r_1^2}{4\bar{t}_1}\right), \quad (23)$$

where n_0 and n_1 are, respectively, the (equilibrium) numbers of the particles in the free-diffusion and trapped states, which are measured directly from the particle trajectories. The effective diffusion coefficient D_1 in the trapped state is estimated as $D_1 = r_1^2/(4\bar{t}_1)$. Figure 9 shows a comparison between the measured D_L and calculated $(D_L)_A$ using Eq. (23) for five colloidal samples. It is seen that the calculated $(D_L)_A$ agrees well with the measured D_L, indicating that the two-state diffusion model discussed in Sec. II A catches the essential physics for the long-time behaviour of colloidal diffusion in the system.

B. Diffusion dynamics on a quasicrystalline lattice

To further understand how the spatial location of the holes on the quasicrystalline lattice affects the overall diffusion of the particles, we consider the probability density function $P(\Delta\mathbf{r}(\tau)|\mathbf{R}_m)$ for a particle to move a distance $\Delta\mathbf{r}$ over a time period τ when it starts from $\mathbf{R}_m$ (the center of the mth trap). As mentioned in Sec. II B, $P(\Delta\mathbf{r}(\tau)|\mathbf{R}_m)$ depends on both the starting site $\mathbf{R}_m$ and displacement vector $\Delta\mathbf{r}(\tau)$ for a quasicrystal. To reduce the statistical complexities of $P(\Delta\mathbf{r}(\tau)|\mathbf{R}_m)$ and improve the measurement statistics, we introduce a spatial average to $P(\Delta\mathbf{r}(\tau)|\mathbf{R}_m)$ over all the starting sites $\mathbf{R}_m$,

$$P(\Delta\mathbf{r}(\tau)|\mathbf{R}_0) \equiv \frac{1}{M}\sum_m^M P(\Delta\mathbf{r}(\tau)|\mathbf{R}_m), \quad (24)$$

where $\mathbf{R}_0$ denotes a generic starting position at the center of the traps, and thus $P(\Delta\mathbf{r}(\tau)|\mathbf{R}_0)$ becomes independent of m.

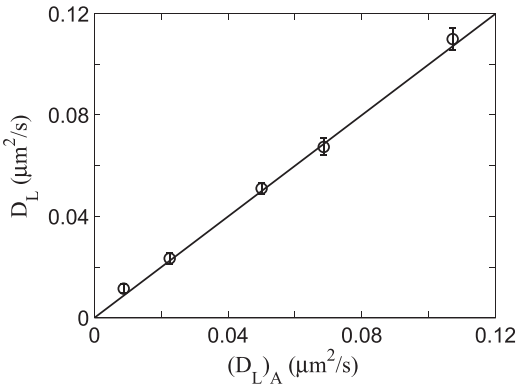

FIG. 9. Comparison between the measured long-time diffusion coefficient D_L and calculated $(D_L)_A$ using Eq. (23) for five colloidal samples. The error bars show the standard deviation of the measured D_L. The solid line shows the equation $D_L = (D_L)_A$.

Figure 10(a) shows the measured $P(\Delta\mathbf{r}(\tau)|\mathbf{R}_0)$ for sample S4. The measurements are made at a long delay time $\tau = 350$ s, which is about 7 times larger than the mean dwell time $\bar{t}_1$ in the trapped state. The measured $P(\Delta\mathbf{r}(\tau)|\mathbf{R}_0)$ reveals high probability spots, which coincide with the position of the neighbouring traps and have a 10-fold rotational symmetry. This 10-fold rotational symmetry can be explained by the fivefold rotational symmetry of the underlying quasicrystalline substrate together with a reflection symmetry between $\mathbf{R}_0$ and $-\mathbf{R}_0$ for the neighbouring pair of traps. Figure 10(a) thus confirms that the measured $P(\Delta\mathbf{r}(\tau)|\mathbf{R}_0)$ retains the essential symmetry of the quasicrystal and removes the minor differences among different sites of the quasicrystal.

For comparison, we also measure the probability density function $P(\Delta\mathbf{r}(\tau))$ for a particle to move a distance $\Delta\mathbf{r}$ over a time period τ without specifying the starting position $\mathbf{R}_0$. This is equivalent to take a spatial average over all possible starting positions $\mathbf{r}$ on the substrate,

$$P(\Delta\mathbf{r}(\tau)) \equiv \int P(\Delta\mathbf{r}(\tau)|\mathbf{r})f(\mathbf{r})d\mathbf{r}, \quad (25)$$

where $f(\mathbf{r})$ is the (equilibrium) probability distribution of finding a particle at position $\mathbf{r}$ on the substrate. Figure 10(b) shows the measured $P(\Delta\mathbf{r}(\tau))$ for sample S4. The average over the

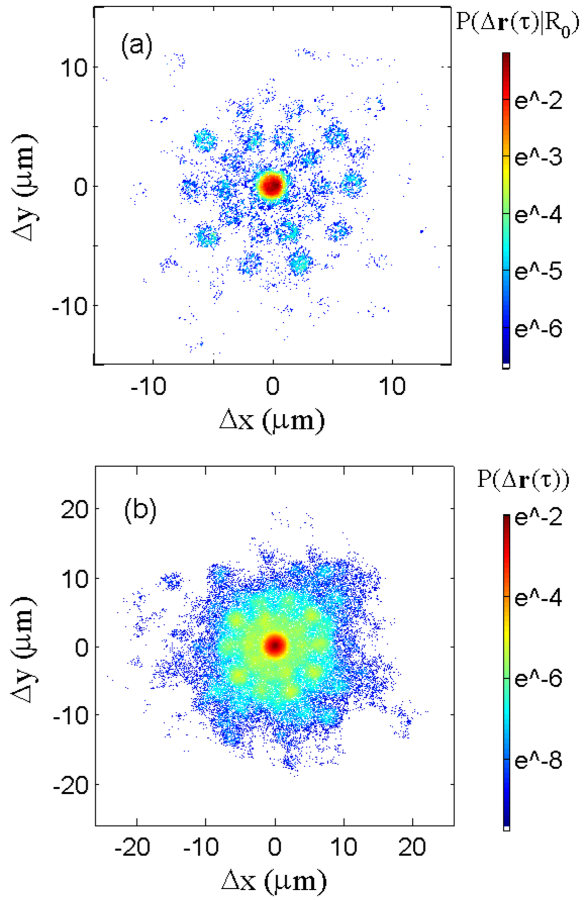

FIG. 10. (a) Measured probability density function $P(\Delta\mathbf{r}(\tau)|\mathbf{R}_0)$ for sample S4. The measurements are made with the starting position $\mathbf{R}_0$ being set at the trap center and delay time $\tau = 350$ s. The color bar is shown in log scale. (b) Measured $P(\Delta\mathbf{r}(\tau))$ for sample S4. The measurements are made without specifying the starting position $\mathbf{R}_0$ and with delay time $\tau = 350$ s. The color bar is shown in log scale.

starting points results in a smeared image of $P(\Delta\mathbf{r}(\tau)|\mathbf{R}_0)$ with the local probability peaks broadened and peak height reduced. Nevertheless, the measured $P(\Delta\mathbf{r}(\tau))$ still retains the 10-fold symmetric pattern with a Gaussian-like envelope. Figure 10(b) thus demonstrates that the measured $P(\Delta\mathbf{r}(\tau))$ is still sensitive to the quasicrystalline structure of the underlying substrate.

To compare the measured D_L with the theoretical prediction given in Eq. (16), we first measure the distribution of the distance ΔR_n between the trapping sites, which is defined in Eq. (15). This is accomplished by counting how many trajectory segments which are directly linked by two trapping sites for any delay time τ. Because of the 10-fold azimuthal symmetry of the measured $P(\Delta\mathbf{r}(\tau)|\mathbf{R}_0)$ as shown in Fig. 10(a), we measure the azimuthally averaged $\Delta R_n \equiv |\Delta\mathbf{R}_n|$ with n indicating the radial position of the nth shell of neighbouring sites away from the trap center. Figure 11 shows the measured histogram $H(\Delta R_n)$ for sample S4. Note that the histogram here records the actual transition path distances of the diffusing particle, which is different from the structural distribution of distances of the quasi-crystalline substrate.[43] Among the observable probability peaks pointed by the arrows, the first three marked peaks contain most of the transition events. These peak locations correspond to the distances, ΔR_1 through ΔR_3, to the first three nearest neighbours. The transition to the farther sites is not forbidden but is found to have much smaller probabilities.

The transition rate between a pair of neighbouring sites is obtained using the equation

$$\Gamma_{m,n} = \frac{M_{m,n}}{M_m}\Gamma_m, \tag{26}$$

where $\Gamma_m = \sum_n \Gamma_{m,n}$ is the total transition rate for a particle to escape from the mth site and arrive at all possible neighbouring sites, $M_{m,n}$ is the number of transitions from the mth site to the nth site, and $M_m = \sum_n M_{m,n}$ is the total number of transitions out of the mth site. The mean transition rate $\langle\Gamma_{m,n}\rangle_m$ in Eq. (16) is given by

$$\langle\Gamma_{m,n}\rangle_m = \left[\frac{\sum_m (M_{m,n}\Gamma_{m,n}^{-1})\Gamma_{m,n}}{\sum_m (M_{m,n}\Gamma_{m,n}^{-1})}\right]\frac{S_n}{S} \equiv \overline{\Gamma}_n \frac{S_n}{S}, \tag{27}$$

where $\Gamma_{m,n}^{-1}$ is the mean transition time for the particle to move from the mth site to the nth site, which is used as a weighting factor to account for the likelihood of occurrence of such transitions with different starting sites m. The time averaged transition rate $\overline{\Gamma}_n$ refers to the transition to a particular kind of neighbouring sites n with the same distance and orientation. As each individual starting site m does not have all the neighbouring sites with a 10-fold symmetry, as shown in Fig. 10, the time averaged transition rate is multiplied by a numerical factor S_n/S to account for the probability of finding a starting site to have the nth kind of neighbours. Here S_n is the number of sites having the nth kind of neighbours and S is the total number of sites. The quantities in Eqs. (26) and (27), including $M_{m,n}$, M_m, Γ_m, S_n, and S, can all be measured directly from the particle trajectories.

The detailed transition dynamics is investigated by examining the local transition rates of the top six most abundant local structural configurations on the quasi-crystalline substrate. Figure 12 shows the six vertex configurations and their transition rates to the neighbouring sites. The mean transition time $(\overline{\Gamma}_n)^{-1}$ is related to the distance ΔR_n between the traps. As the energy barrier E_b for sample S1 is rather small ($\simeq 1\, k_BT$), the transition time is determined primarily by the travelling time between the two traps. A further travelling distance results in a longer transition time because the particle needs a longer time to diffuse to a further distance, which suggests that the transition time goes as ΔR_n^2. In addition, the traps have a finite size, so that the angle of coverage of a targeting trap is proportional to ΔR_n^{-1}, which gives rise to a smaller probability for the particle to arrive at a further targeting trap. Combining these two effects, we find the mean transition time $(\overline{\Gamma}_n)^{-1}$ to be proportional to ΔR_n^3. The transition times $(\overline{\Gamma}_n)^{-1}$ shown in Fig. 12 are measured via Eq. (26) and averaged over all the rotational or/and mirroring symmetric vertices. Within the experimental uncertainties of $\lesssim$14%, the measured $(\overline{\Gamma}_n)^{-1}$ is approximately the same for all the transitions with the same distance regardless of their detailed configurations. For the three nearest transitions among the six most abundant vertices as shown in Fig. 12, their transition distances are, respectively, ℓ_h, $1.618\ell_h$, and $1.902\ell_h$. The measured transition times $(\overline{\Gamma}_n)^{-1}$

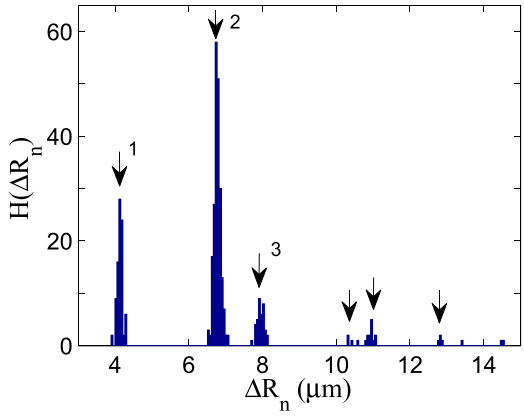

FIG. 11. Measured histogram $H(\Delta R_n)$ of the distance ΔR_n between the trapping sites for sample S4. The arrows point to the probability peaks observed. The first three peaks marked are associated with the distances, ΔR_1 through ΔR_3, to the first three nearest neighbours.

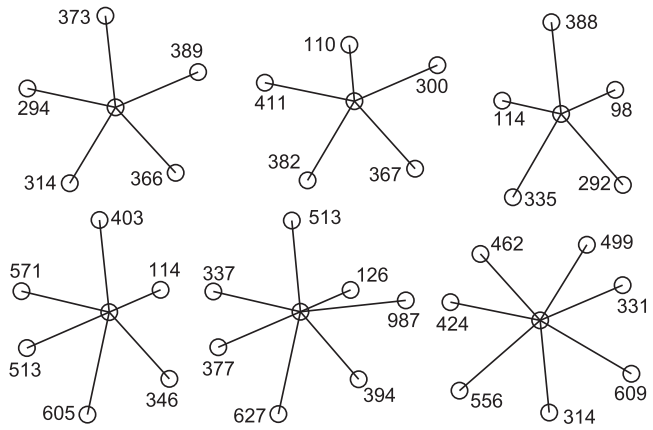

FIG. 12. Measured mean transition times $(\overline{\Gamma}_n)^{-1}$ (numbers marked in seconds) of a selected set of paths in sample S1. The six vertices listed here have the largest population among the 12 vertices as shown in Fig. 2(b).

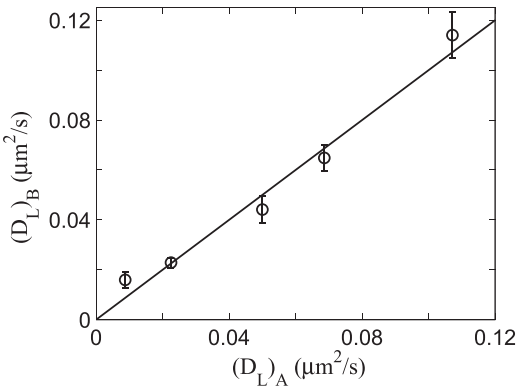

FIG. 13. Comparison between the calculated long-time diffusion coefficients, $(D_L)_B$ using Eq. (16) and $(D_L)_A$ using Eq. (23), for five colloidal samples. The error bars show the experimental uncertainties in determining the values of $(D_L)_B$. The solid line shows the equation $(D_L)_B = (D_L)_A$.

for these three distances are around 110 s, 388 s, and 677 s, respectively, which agree approximately with the relation, $(\overline{\Gamma}_n)^{-1} \propto \Delta R_n^3$, as discussed above.

With the measured ΔR_n and $\langle \Gamma_{m,n} \rangle_m$, we now can use Eq. (16) to calculate $(D_L)_B$. Because the azimuthally symmetric neighbours have the same transition distance, they can be counted together without changing the final result of Eq. (16). Therefore, we carry out the summation over n in Eq. (16) first along the azimuthal direction, which leads to a summation of $\langle \Gamma_{m,n} \rangle_m$ over the nth shell of the nearest neighbours with the same distance ΔR_n, followed by a sum over all the distances ΔR_n, which are shown in Fig. 11. Figure 13 shows a comparison between the calculated long-time diffusion coefficients, $(D_L)_B$ using Eq. (16) and $(D_L)_A$ using Eq. (23), for five colloidal samples. It is seen that the calculated $(D_L)_B$ is in good agreement with $(D_L)_A$.

V. SUMMARY

In this work, we have studied how an array of quasicrystalline traps affect the diffusive motion of non-interacting silica spheres. We obtained a large volume of single particle trajectories for five samples with different particle diameters d_p and different quasicrystalline substrates with varying hole diameters d_h and shortest distances ℓ_h between the holes (see Table I). The particle trajectories show two distinct states: a trapped state when the particles are inside the holes and a free-diffusion state when they are outside the holes. From the measured particle trajectories, we also obtained the potential $U(x, y)$ of the trapping holes felt by the particles and the barrier height E_b of the traps is found to be in the range 1-6 k_BT.

To describe the colloidal diffusion between the two states, we measured the histograms, $H(t_1)$ of the dwell time t_1 in the trapped state and $H(t_0)$ of the dwell time t_0 in the free-diffusion state, and the mean squared displacement (MSD) $\langle \Delta \mathbf{r}^2(\tau) \rangle$ in the two states, from which we obtained the free diffusion coefficient D_0 and trap size r_1. The measured MSD curves of the full trajectories for different samples exhibit a dual-crossover behaviour with an initial short-time diffusion followed by a crossover to the subdiffusion regime caused by temporary trapping of the particles by the holes on the substrate. When the delay time τ becomes longer than the dwell time t_1, the particles on average have escaped from the potential traps and their motion is changed back to diffusion again with the measured MSD curves being linear in τ, from which we obtained the long-time diffusion coefficient D_L.

Two theoretical models were developed to describe the long-time diffusion of the colloidal particles. The first model considers the particle motion in the two states as two diffusion processes with different diffusion coefficients, and the spatial arrangement of the traps is ignored by assuming that the transition rates between the two states are constant over the entire space. By solving the coupled diffusion equations, we obtained an analytical solution of the long-time diffusion coefficient $(D_L)_A$ [given in Eq. (23)], which is found in good agreement with the measured D_L.

The second model considers the particle motion as a hopping on a quasicrystalline network. Because every site in a quasicrystal is different from each other,[27] it is difficult to have an exact solution for this model. Nonetheless, we find that by taking an average over all the starting sites, the measured transition probability density function $P(\Delta \mathbf{r}(\tau)|\mathbf{R}_0)$ has 10-fold rotational symmetry [Fig. 10(a)], which is directly linked to the quasicrystalline structure of the substrate. By applying this averaging approach to the transition rate $\Gamma_{m,n}$, we obtained an analytical solution of the long-time diffusion coefficient $(D_L)_B$ [given in Eq. (16)], which is in good agreement with both the calculated $(D_L)_A$ based on the first model and measured D_L.

Both models are valid in the long-time regime when the particles travel a distance longer than the mean separation between the nearest traps, so that their dynamics becomes statistically homogeneous. Under this circumstance, our coarse-grained approach provides a useful way to describe the long-time diffusion using the characteristic local properties of the diffusing particles, such as their local diffusion coefficients or transition rates, which can be accurately measured in the experiment. These two models can also be generalized to the situations with periodic or even randomly distributed traps, so long as the distribution of the traps is homogeneous. But in general one of the models may work better than the other. For example, in the situation with densely packed traps, such as atom diffusion on a solid surface, the traps are contiguous and thus the first model might not be applicable since there is no clearly free-diffusion state between the traps. At the other limit of sparse traps, such as diffusion in a homogeneous material with a few trapping defects, the transitions between traps may not be easily quantified as simple Poisson jumps with a constant transition rate. In this case, the first model is more suitable than the second model. Overall, this study provides new insights into our general understanding and analysis techniques for colloidal diffusion over complex potential landscapes.

ACKNOWLEDGMENTS

This work was supported in part by RGC of Hong Kong SAR under Grant Nos. A-HKUST616/14-A (Y.H. and P.T.) and HKUST16302816 (P.T.) and by the MoST of Taiwan under Grant No. 104-2112-M-008-003-MY3 (P.Y.L.).

[1]J. W. Haus and K. W. Kehr, "Diffusion in regular and disordered lattices," Phys. Rep. **150**, 263 (1987).
[2]J. P. Bouchaud and A. Georges, "Anomalous diffusion in disordered media: Statistical mechanisms models and physical applications," Phys. Rep. **195**, 127 (1990).
[3]S. Havlin and D. Ben-Avraham, "Diffusion in disordered media," Adv. Phys. **51**(1), 187 (2002); Originally published in, Adv. Phys. **36**, 695 (1987).
[4]S. J. Harris, A. Timmons, D. R. Baker, and C. Monroe, "Direct *in situ* measurements of Li transport in Li-ion battery negative electrodes," Chem. Phys. Lett. **485**, 265–274 (2010).
[5]A. Kusumi, Y. Umemura, N. Morone, and T. Fujiwara, "Paradigm shift of the molecular dynamics concept in the cell membrane: High-speed single-molecule tracking revealed the partitioning of the cell membrane," in *Anomalous Transport: Foundations and Applications*, edited by R. Klages, G. Radons, and I. M. Sokolov (Wiley-VCH Verlag GmbH & Co. KGaA, Weinheim, Germany, 2008), Chap. 19, pp. 545–574.
[6]K. Ritchie, X. Y. Shan, J. Kondo, K. Iwasawa, T. Fujiwara, and A. Kusumi, "Detection of non-Brownian diffusion in the cell membrane in single molecule tracking," Biophys. J. **88**, 2266–2277 (2005).
[7]A. V. Weigel, B. Simon, M. M. Tamkun, and D. Krapfa, "Ergodic and nonergodic processes coexist in the plasma membrane as observed by single-molecule tracking," Proc. Natl. Acad. Sci. U. S. A. **108**, 6438–6443 (2011).
[8]I. Golding and E. C. Cox, "Physical nature of bacterial cytoplasm," Phys. Rev. Lett. **96**, 098102 (2006).
[9]W. He, H. Song, Y. Su, L. Geng, B. J. Ackerson, H. B. Peng, and P. Tong, "Dynamic heterogeneity and non-Gaussian statistics for acetylcholine receptors on live cell membrane," Nat. Commun. **7**, 11701 (2016).
[10]F. Zhang, G. M. Lee, and K. Jacobson, "Protein lateral mobility as a reflection of membrane microstructure," BioEssays **15**, 579 (1993).
[11]K. Jacobson, E. D. Sheets, and R. Simson, "Revisiting the fluid mosaic model of membranes," Science **268**, 1441 (1995).
[12]D. M. Engelman, "Membranes are more mosaic than fluid," Nature **438**, 578–580 (2005).
[13]M. L. Kraft, "Plasma membrane organization and function: Moving past lipid rafts," Mol. Biol. Cell **24**, 2765–2768 (2013).
[14]E. Barkai, Y. Garini, and R. Metzler, "Strange kinetics of single molecules in living cells," Phys. Today **65**(8), 29 (2012).
[15]F. Hofling and T. Franosch, "Anomalous transport in the crowded world of biological cells," Rep. Prog. Phys. **76**, 046602 (2013).
[16]R. L. Baldwin, "Matching speed and stability," Nature **369**, 183 (1994).
[17]R. L. Baldwin, "The nature of protein folding pathways: The classical versus the new view," J. Biomol. NMR **5**, 103 (1995).
[18]Y. Meroz and I. M. Sokolov, "A toolbox for determining subdiffusive mechanisms," Phys. Rep. **573**, 1–29 (2015).
[19]S. Lifson and J. L. Jackson, "On the self-diffusion of ions in a polyelectrolyte solution," J. Chem. Phys. **36**, 2410 (1962).
[20]K. W. Kehr, D. Richter, and R. H. Swendsen, "The influence of impurities on interstitial diffusion," J. Phys. F: Met. Phys. **8**, 433 (1978).
[21]P. J. H. Denteneer and M. H. Ernst, "Exact results for diffusion on a disordered chain," J. Phys. C: Solid State Phys. **16**, L961 (1983).
[22]P. J. H. Denteneer and M. H. Ernst, "Diffusion in systems with static disorder," Phys. Rev. B **29**, 1755 (1984).
[23]R. Zwanzig, "Non-Markoffian diffusion in a one-dimensional disordered lattice," J. Stat. Phys. **28**, 127 (1982).
[24]H. Scher and M. Lax, "Stochastic transport in a disordered solid. I. Theory," Phys. Rev. B **7**, 4491 (1973).
[25]A. Lubelski, I. M. Sokolov, and J. Klafter, "Nonergodicity mimics inhomogeneity in single particle tracking," Phys. Rev. Lett. **100**, 250602 (2008).
[26]R. Metzler and J. Klafter, "The random walk's guide to anomalous diffusion: A fractional dynamics approach," Phys. Rep. **339**, 1 (2000).
[27]D. Levine and P. J. Steinhardt, "Quasicrystals. I. Definition and structure," Phys. Rev. B **34**, 596–616 (1986).
[28]J. E. S. Socolar and P. J. Steinhardt, "Quasicrystals. II. Unit-cell configurations," Phys. Rev. B **34**, 617–647 (1986).
[29]M. Schmiedeberg, J. Roth, and H. Stark, "Brownian particles in random and quasicrystalline potentials: How they approach the equilibrium," Eur. Phys. J. E **24**, 367–377 (2007).
[30]A. S. Kraemer and D. P. Sanders, "Periodizing quasicrystals: Anomalous diffusion in quasiperiodic systems," preprint arXiv: 1206.1103 (2012).
[31]F. Samavat, M. J. Gladys, C. J. Jenks, T. A. Lograsso, B. V. King, and D. J. O'Connor, "Surface layer self diffusion in icosahedral Al-Pd-Mn quasicrystals," Surf. Sci. **601**, 5678–5682 (2007).
[32]L. Guidoni, B. Dépret, A. di Stefano, and P. Verkerk, "Atomic diffusion in an optical quasicrystal with five-fold symmetry," Phys. Rev. A **60**, R4233–R4236 (1999).
[33]J. E. Socolar, P. J. Steinhardt, and D. Levine, "Quasicrystals with arbitrary orientational symmetry," Phys. Rev. B **32**(8), 5547 (1985).
[34]X. G. Ma, P. Y. Lai, and P. Tong, "Colloidal diffusion over a periodic energy landscape," Soft Matter **9**, 8826 (2013).
[35]X. G. Ma, P. Y. Lai, B. J. Ackerson, and P. Tong, "Colloidal transport and diffusion over a tilted periodic potential: Dynamics of individual particles," Soft Matter **11**, 1182 (2015).
[36]J. C. Crocker and D. G. Grier, "Methods of digital video microscopy for colloidal studies," J. Colloid Interface Sci. **179**, 298 (1996).
[37]P. Hanggi, P. Talkner, and M. Borkovec, "Reaction-rate theory: Fifty years after Kramers," Rev. Mod. Phys. **62**, 251 (1990).
[38]R. D. L. Hanes, C. Dalle-Ferrier, M. Schmiedeberg, M. C. Jenkinsa, and S. U. Egelhaaf, "Colloids in one dimensional random energy landscapes," Soft Matter **8**, 2714 (2010).
[39]F. Evers, C. Zunke, R. D. L. Hanes, J. Bewerunge, I. Ladadwa, A. Heuer, and S. U. Egelhaaf, "Particle dynamics in two-dimensional random-energy landscapes: Experiments and simulations," Phys. Rev. E **88**, 022125 (2013).
[40]A. Ghosh, V. Chikkadi, P. Schall, and D. Bonn, "Connecting structural relaxation with the low frequency modes in a hard-sphere colloidal glass," Phys. Rev. Lett. **107**, 188303 (2011).
[41]G. L. Hunter and E. R. Weeks, "The physics of the colloidal glass transition," Rep. Prog. Phys. **75**, 066501 (2012).
[42]I. Y. Wong, M. L. Gardel, D. R. Reichman, E. R. Weeks, M. T. Valentine, A. R. Bausch, and D. A. Weitz, "Anomalous diffusion probes microstructure dynamics of entangled F-actin networks," Phys. Rev. Lett. **92**, 178101 (2004).
[43]From the structure of the quasi-crystalline substrate as shown in Fig. 2(b), we find the relative abundance of the nearest neighbour trap separation to that of the second nearest neighbour and the third nearest neighbour to be about 1:5:1.9.